Title:	**Structural Performance of 800 MPa High-Strength Steel Members**
Author:	Cheol H. Lee, Department of Architecture and Architectural Engineering, Seoul National University
Subject:	Structural Engineering
Keywords:	Seismic Steel Structural Engineering
Publication Date:	2017
Original Publication:	International Journal of High-Rise Buildings Volume 6 Number 3
Paper Type:	1. Book chapter/Part chapter 2. **Journal paper** 3. Conference proceeding 4. Unpublished conference paper 5. Magazine article 6. Unpublished

International Journal of High-Rise Buildings
September 2017, Vol 6, No 3, 249-259
https://doi.org/10.21022/IJHRB.2017.6.3.249

International Journal of
High-Rise Buildings
www.ctbuh-korea.org/ijhrb/index.php

Structural Performance of 800 MPa High-Strength Steel Members and Application to Highrise and Mega Building Structures

Cheol-Ho Lee†

Department of Architecture and Architectural Engineering, Seoul National University, Seoul 08826, Korea

Abstract

The use of high-strength steels in construction of highrise and mega building structures can bring about many technological advantages from fabrication to erection. However, key design criteria such as local and lateral stability in current steel design specifications were developed based on tests of ordinary steels which have stress-strain characteristics very different from that of high strength steels. A series of tests on 800 MPa tensile strength steel (HSA800) members are summarized in this paper which were conducted to investigate the appropriateness of extrapolating current ordinary-steel based design criteria to high strength steels. 800 MPa I-shape beam specimens designed according to flange local buckling (FLB) criteria of the AISC Specification developed a sufficient strength for elastic design and a marginal rotation capacity for plastic design. It is shown that, without introducing distinct and significant yield plateau to the stress-strain property of high-strength steel, it is inherently difficult to achieve a high rotation capacity even if all the current stability limits are met. 800 MPa I-shape beam specimens with both low and high warping rigidity exhibited sufficient lateral torsional buckling (LTB) strength. HSA800 short-column specimens with various edge restraint exhibited sufficient local buckling strength under uniform compression and generally outperformed ordinary steel specimens. The experimental *P-M* strength was much higher than the AISC nominal *P-M* strength. The measured residual stresses indicated that the impact of residual stress on inelastic buckling of high-strength steel is less. Cyclic seismic test results showed that HSA800 members have the potential to be used as non-ductile members or members with limited ductility demand in seismic load resisting systems. Finally, recent applications of 800 MPa high strength steel to highrise and mega building structures in Korea are briefly presented.

Keywords: High-strength steel, Stability criteria, Buckling, Rotation capacity, Ductility, Seismic

1. Introduction

The use of high-strength steels in construction of high-rise and mega building structures can bring about many technological advantages from fabrication to erection. For example, smaller sections made of high-strength steel can enhance space availability, aesthetics, and freedom in design as well. The benefits of high-strength steels combined with economical steel making have stimulated a great interest in developing high-strength steels for use in building and bridge applications in Korea. Recently two types of high-strength steels, HSB800 and HSA800, with a nominal tensile strength of 800 MPa were developed in Korea for bridge and building applications, respectively. Table 1 summarizes the material specifications for both steels.

However, high-strength steels have different stress-strain characteristics and often need more careful technical considerations in terms of ductility and weldability. Key design criteria such as local and lateral stability in current steel design specifications were developed based on tests of ordinary steels whose stress-strain characteristics is very different from that of high strength steels. Ordinary steels have stress-strain characteristics desirable for ductile behavior at member and structural levels; they have a sharp yield point, a distinct yield plateau, significant strain-hardening, and a low yield ratio. However, high-strength steels lack these properties (see Fig. 1), which is perhaps the key reason for some past studies (McDermott 1969; Ricles et al. 1998; Green 2000). The author conducted a

Table 1. Material specifications for HSB800 and HSA800

Items	HSB800	HSA800
Yield ratio	N/A	Max. 0.85
Yield strength (MPa)	Min. 690	650~770
Tensile strength (MPa)	Min. 800	800~950
Plate thickness available (mm)	Max. 80	25~100
Charpy V-notch toughness	47J@-20?	47J@-5?
Elongation (%)	Min. 15	Min. 15
Carbon equivalent (CE) (%)	Max. 0.55	Max. 0.6

†Corresponding author: Cheol-Ho Lee
Tel: +82-2-880-9061; Fax: +82-2-878-9061
E-mail: ceholee@snu.ac.kr

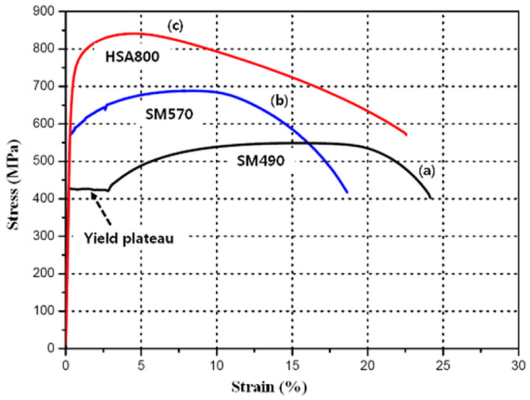

Figure 1. Typical stress-strain curves of various grades of steel.

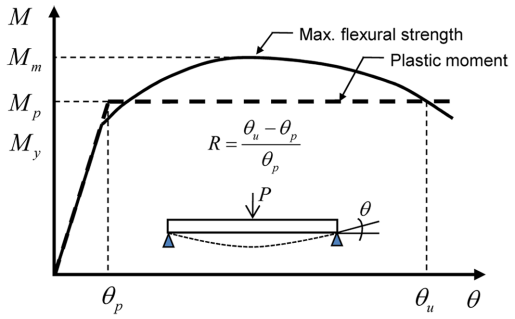

Figure 2. Definition of rotation capacity of flexural member.

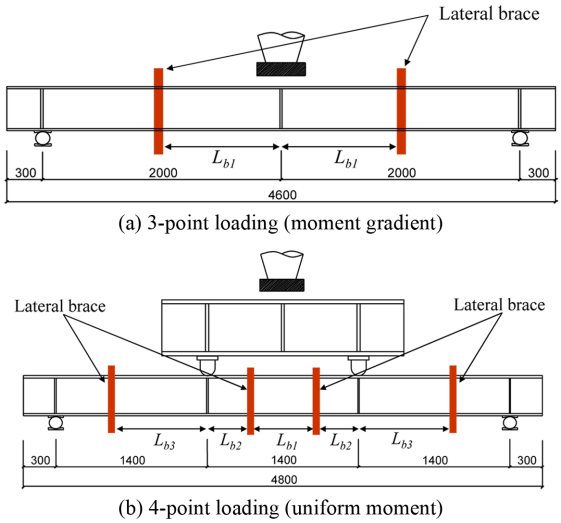

Figure 3. Loading conditions and lateral bracing.

series of experimental and analytical studies to investigate if current ordinary-steel based design criteria are also applicable to 800 MPa steel members from both strength and ductility perspectives (for example, Lee el al., 2013; Park et al., 2013; Kim et al., 2014). The key results from these previous studies and recent application examples of 800 MPa steel in Korea are briefly presented in this paper.

2. Test on Flange Local Buckling

2.1. Design of Test Specimens

The ductility of a flexural member is generally measured in terms of the rotation capacity, R (see Fig. 2).

$$R=\frac{\theta_u-\theta_p}{\theta_p}=\frac{\theta_u}{\theta_p}-1 \quad (1)$$

where θ_p = hypothetical beam end rotation at which the moment first reaches M_p, θ_u = beam end rotation at which the moment reaches M_p after reaching a maximum moment M_m. The limit states affecting the rotation capacity include local buckling, lateral-torsional buckling, tensile fracture, and plastic yielding.

For specimen design purposes, all the current stability (local and lateral buckling) criteria were assumed to be still applicable to high-strength steel. Full-scale I-shaped beam specimens were fabricated by using SM490, HSB 800, and HSA800 steels. Full-scale I-shaped beam specimens were fabricated by using SM490, HSB800, and HSA800 steels. See Table 2 for the test matrix. The benchmark specimens made of ordinary steel SM490 (similar to A572 Gr. 50) were also included for comparison purposes. Tests were conducted in two phases. Beams with HSB800 and SM490 steels were tested in Phase I while HSA800 steel beams were tested in Phase II. In this testing program the key test variable was the flange width-thickness ratio.

Seismically compact webs were used to minimize the interaction between flange and web local buckling. Sufficient lateral bracing was also provided to avoid lateral-torsional buckling of the beam. Fig. 3 shows the loading schemes and lateral bracing. Both the 3- and 4-point loading schemes were used to investigate the effect of moment gradient on beam behavior. The standard symbols of the AISC Specification are used in this paper.

2.2. Flexural Strength and Rotation Capacity Observed

Depending on the plastic deformation capacity required, structural steel design can be classified into three categories: elastic, plastic, and seismic design (Galambos et al., 1997). In elastic design, members of a structure are assumed to remain essentially elastic. On the other hand, for plastic design a rotation capacity of approximately 3 is implied in the AISC Specification to achieve the mechanism strength through moment redistribution in a statically indeterminate structure. The AISC Specification forbids the use of steel material with a yield stress higher than 450 MPa for plastic design because of concerns about its low plastic deformation capacity. In seismic design, a minimum rotation capacity of about 7 has been implied for

Table 2. Test matrix

Test program	Specimen designation	Steel	Depth H (mm)	Width b_f (mm)	Web thickness t_w (mm)	Flange thickness t_f (mm)	Width-thickness ratio λ		Beam span L (mm)
							Flange	Web	
Phase I	SM490-S-LPD-3	SM 490	399	500	11.0	11.0	22.7	34.4	4,000
	SM490-C-LPD-3-A		400	219	11.0	12.0	9.1	34.2	4,000
	SM490-C-LPD-3-B		400	220	11.0	15.0	7.3	33.6	4,000
	SM490-C-LP-4		400	219	11.0	12.0	9.1	34.2	4,200
	SM490-C-LPD-4		400	218	11.0	12.0	9.1	34.2	4,200
	HSB800-NC-LP-3	HSB 800	400	500	17.6	17.6	14.2	20.7	3,500
	HSB800-NC-LPD-3		400	220	17.6	17.6	6.3	20.7	4,000
	HSB800-C-LPD-3		400	220	17.6	21.1	5.2	20.3	4,000
	HSB800-NC-LP-4-A		400	220	17.6	17.6	6.3	20.7	4,200
	HSB800-NC-LP-4-B		400	220	17.6	17.6	6.3	20.7	4,200
Phase II	HSA800-S-LPD-3-FHS	HSA 800	400	650	17.6	17.6	18.5	20.7	4,000
	HSA800-NC-LPD-3-PHS		400	240	17.6	15.0	8.0	21.0	4,000
	HSA800-NC-LPD-3-FHS		401	238	17.6	15.0	7.9	21.1	4,000
	HSA800-C-LPD-3-PHS		400	201	17.6	20.0	5.0	20.5	4,000
	HSA800-C-LPD-3-FHS		399	200	17.6	20.0	5.0	20.4	4,000
	HSA800-C-LP-3-PHS		400	199	17.6	20.0	5.0	20.5	4,000
	HSA800-SC-LPD-3-PHS		400	160	17.6	20.0	4.0	20.5	4,000
	HSA800-SC-LPD-3-FHS		400	160	17.6	20.0	4.0	20.5	4,000
	HSA800-NC-LP-4-PHS		400	241	17.6	15.0	8.0	21.0	4,200
	HSA800-NC-LP-4-FHS		400	240	17.6	15.0	8.0	21.0	4,200
	HSA800-C-LP-4-PHS		400	199	17.6	20.0	4.0	20.5	4,200

Note: SC= seismically compact; C= compact; NC= non-compact; S= slender; LP, LPD= lateral brace for plastic strength and plastic design, respectively; 3= three point loading; 4= four point loading (see Figure 3); FHS= full height stiffener; PHS= partial height stiffener.

high seismic applications following Chopra and Newmark (1980). In the following, test results are analyzed from the perspective of these design methods.

Table 3 summarizes the maximum flexural strength (M_m), the rotation capacity (R), and the failure mode. The plastic moment M_p was calculated using the measured cross section dimensions and yield stress. For beams with non-compact or slender flanges, the maximum moment was also normalized by M_n, which was computed based on the AISC Specification with the measured yield stress. As can be seen from Table 3, all the SM490 specimens showed sufficient flexural strength and rotation capacity. For example, SM490-C-LPD-3-A/B developed a rotation capacity as high as about 10. The performance of 800 MPa specimens was also satisfactory from the strength perspective; even the specimens with non-compact flanges developed the plastic moment, and the majority of them were able to develop a rotation capacity of about 1.5 to 2.0. HSA800 specimens designed per the plastic design criterion was able to develop a rotation capacity exceeding 3. Generally, the effects of flange slenderness, moment gradient, and lateral bracing on flexural strength and rotation capacity were much less pronounced in the 800 MPa specimens than in the SM490 specimens (refer to Lee et al., 2013 for more detailed discussions).

2.3. Effect of Stress-Strain Characteristics on Rotation Capacity Effect of Stress-Strain Characteristics on Rotation Capacity

For beams with a compact section and properly braced, Table 3 shows that SM490 (or ordinary) steel beams had a much higher rotation capacity than their high-strength steel counterpart. In addition, the flexural overstrength, m (= M_m/M_p) is also higher for ordinary-steel beams. The lower rotation capacity and flexural overstrength of the 800 MPa beams are mainly due to the unique stress-strain characteristics. Refer to Fig. 4 for a simply supported beam with the maximum moment developed. Given the moment diagram and the associated stress-strain relationships, the simplified curvature distributions along half of the beam span are shown in Figs. 4(b) and 4(c) for ordinary steel and high-strength steel, respectively. Because ordinary steel shows a distinct yield plateau, the strain jump from ε_y to ε_{sh} also produces a jump of curvature, $(s\text{-}1)\phi_p$, in the inelastic region (Lay, 1965b; McDermott, 1969). According to the curvature-area method, the area under the curvature diagram represents the beam end rotation. But the strain jump does not exist in high-strength steel. Therefore, the plastic portion of the beam end rotation (θ_p) produced by strain jump (i.e., the shaded area in Fig. 4b) is much lower for high-strength steel beams. A lack of a clearly defined yield plateau and low strain hardening in the 800 MPa

Table 3. Summary of flexural strength, rotation capacity, and failure modes

Test program	Specimen designation	Section class	Normalized strength		R		Failure mode
			M_m/M_p	M_m/M_n	Target	test	
Phase I	SM490-S-LPD-3	Slender	0.86	1.69	-	-	Local buckling
	SM490-C-LPD-3-A	Compact	1.34	-	3.0	9.5	Local buckling
	SM490-C-LPD-3-B	Compact	1.28	-	3.0	10.1	Local buckling
	SM490-C-LP-4	Compact	1.20	-	-	4.3	Local and lateral buckling
	SM490-C-LPD-4	Compact	1.21	-	3.0	5.5	Local and lateral buckling
	HSB800-NC-LP-3	Non-compact	0.99	1.55	-	-	Local buckling
	HSB800-NC-LPD-3	Non-compact	1.14	1.19	-	0.9	Tensile fracture
	HSB800-C-LPD-3	Compact	1.21	-	3.0	1.9	Tensile fracture
	HSB800-NC-LP-4-A	Non-compact	1.07	1.11	-	2.0	Lateral buckling
	HSB800-NC-LP-4-B	Non-compact	1.12	1.16	-	1.9	Tensile fracture
Phase II	HSA800-S-LPD-3-FHS	Slender	0.82	2.04	-	-	Local buckling
	HSA800-NC-LPD-3-PHS	Non-compact	1.06	1.19	-	2.1	Local buckling
	HSA800-NC-LPD-3-FHS	Non-compact	1.07	1.20	-	1.8	Tensile fracture
	HSA800-C-LPD-3-PHS	Compact	1.10	-	3.0	3.6	Local buckling
	HSA800-C-LPD-3-FHS	Compact	1.12	-	3.0	3.5	Tensile fracture
	HSA800-C-LP-3-PHS	Compact	1.10	-	-	3.1	Local buckling
	HSA800-SC-LPD-3-PHS	Seismic compact	1.12	-	7.0	2.7	Local and lateral buckling
	HSA800-SC-LPD-3-FHS	Seismic compact	1.14	-	7.0	3.1	Local buckling and Tensile fracture
	HSA800-NC-LP-4-PHS	Non-compact	1.07	1.20	-	1.9	Local and lateral buckling
	HSA800-NC-LP-4-FHS	Non-compact	1.07	1.20	-	1.6	Local and lateral buckling
	HSA800-C-LP-4-PHS	Compact	1.07	-	-	2.0	Local and lateral buckling

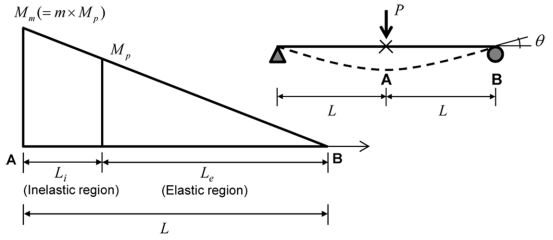

(a) Deflection shape and bending moment diagram

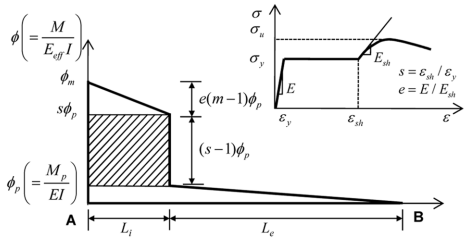

(b) Curvature distribution of ordinary steel beam

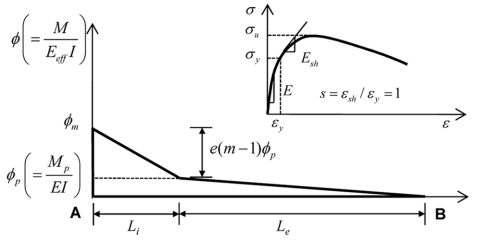

(c) Curvature distribution of high-strength steel beam

Figure 4. Simplified curvature distribution with a moment gradient.

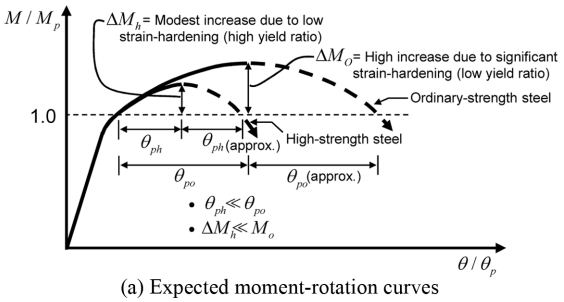

(a) Expected moment-rotation curves

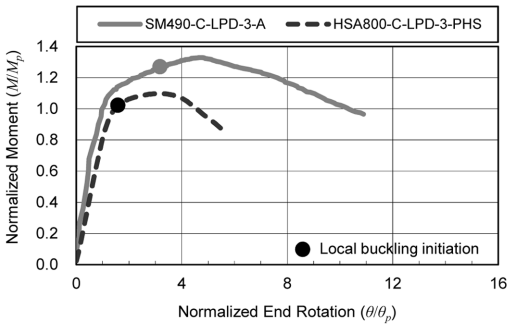

(b) Moment-rotation curves of tested specimens

Figure 5. Effect of stress-strain characteristics on moment-rotation curves.

steel results in a high yield ratio and, hence, a lower flexural overstrength of the beam. Therefore, the expected moment-rotation relationships for both ordinary- and high-

Table 4. Section information and key properties

	Specimen	S1~S3 (Group A)	S4~S6 (Group B)
Section properties	(1) Dimension ($d\times b\times t_w\times t_f$)	H-250×150×15×15	H-400×150×15×15
	(2) Lateral bending constant, I_y (mm^4)	8,499,375	8,541,563
	(3) Warping constant, C_w (mm^6)	116,490,234,375	312,622,109,375
	(4) Torsional constant, J (mm^4)	601,875	770,625
	(5) Flange slenderness, $b/2t_f$	5.0 (6.2)[a]	5.0 (6.2)[a]
	(6) Web slenderness, h/t_w	15.0 (64.0)[a]	25.0 (64.0)[a]

[a]Width-to-thickness ratio limits for compact section (per AISC Specification).

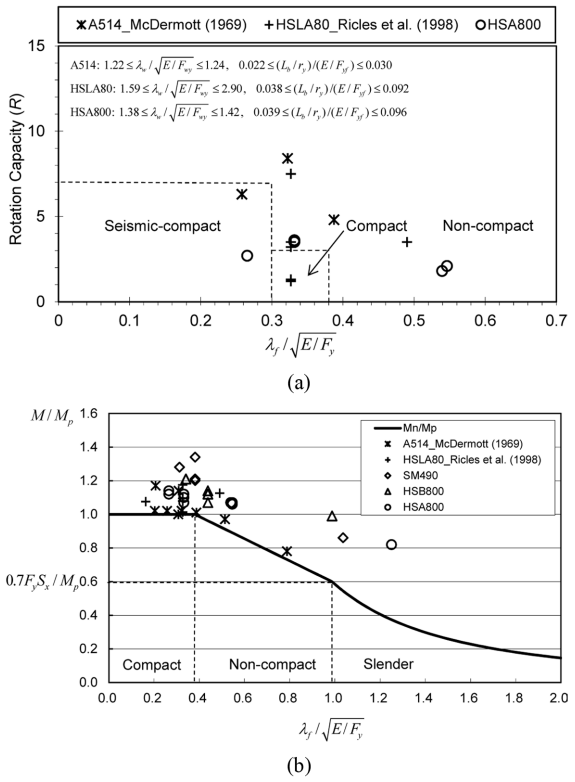

(a)

(b)

Figure 6. Effect of flange slenderness on rotation capacity and comparison of tested flexural strength with nominal strength curve.

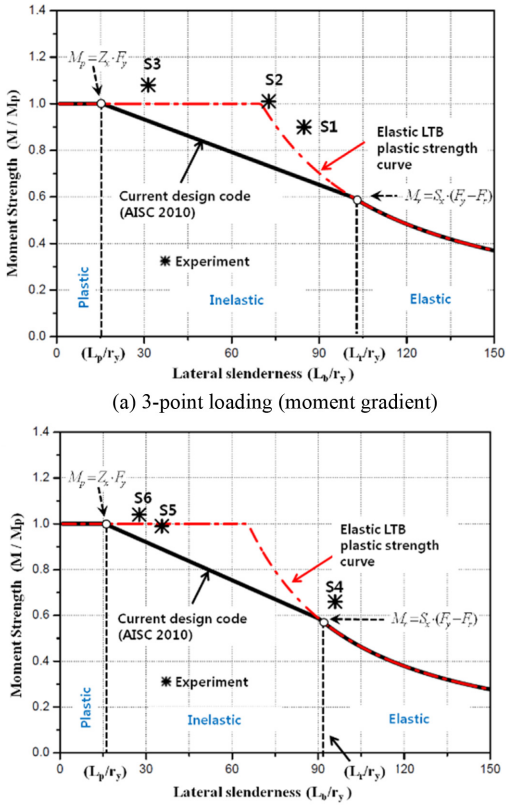

(a) 3-point loading (moment gradient)

(b) 4-point loading (uniform moment)

Figure 7. Comparison of experimental and nominal LTB strength.

strength steels are depicted in Fig. 5(a), where the plastic rotations before and after the maximum moment is reached are assumed to be equal (Kemp 1996). This predicted trend is consistent with the test results shown in Fig. 5(b). Based on Table 3, it appears difficult for 800 MPa steel to achieve a rotation capacity higher than 3.5 even if stringent local and lateral buckling limit states are met.

2.4. Comparison with Existing Test Results

Test data that showed either local buckling or tensile fracture from the tests on high-strength steel beams by McDermott (1969) and Ricles et al. (1998) were compared with results from this study. All the high-strength steel beams in Fig. 6 did not meet the requirements implied for high seismic application (R>7). As presented in Fig. 6(b), all high-strength specimens satisfied the AISC strength requirement. The member flexural overstrength becomes larger as the flange slenderness increases. The reason for the large flexural overstrength observed in the slender or almost slender specimens under moment gradient was explained in detail in the previous study (Lee et al., 2013). Recently, more exact formula to predict local buckling strength of slender flange was proposed by Han and Lee (2016).

3. Test on Lateral Torsional Buckling

3.1. Design of Test Specimens

Inelastic lateral-torsional buckling (LTB) strength of

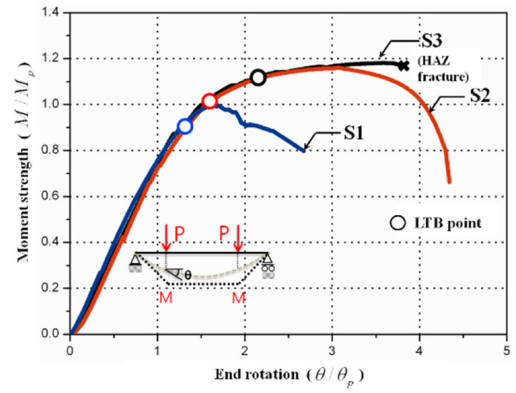

(a) 3-point loading (moment gradient)

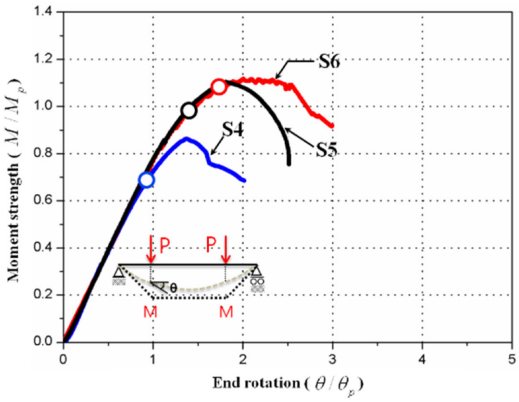

(b) 4-point loading (uniform moment)

Figure 8. Bending moment versus end rotation curves observed.

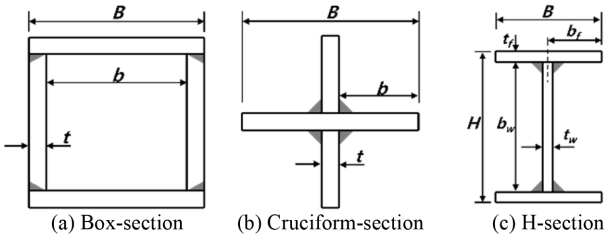

(a) Box-section (b) Cruciform-section (c) H-section

Figure 9. Specimen cross sections for concentric load tests.

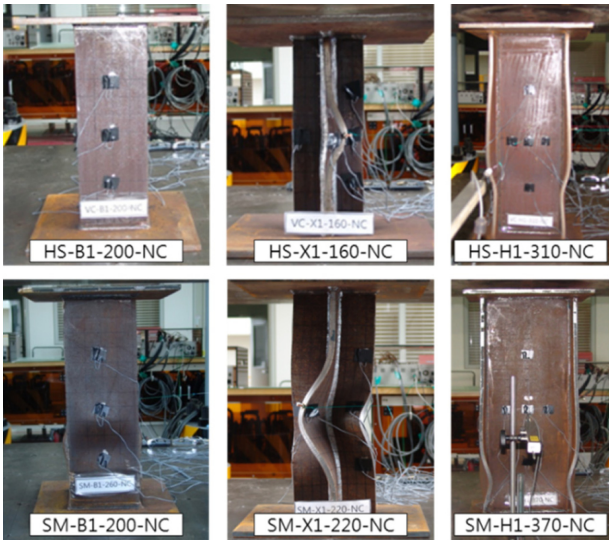

Figure 10. Typical buckling modes of concentric load test specimens.

high-strength H-beams built up from HSA800 steel was experimentally and analytically evaluated in the previous study (Park and Lee, 2013). Again, the motivation was to evaluate whether current AISC LTB provisions, which were originally developed for ordinary steels, are still applicable to high-strength steel. Two sets of compact-section specimens with relatively low (Group A) or high (Group B) warping stiffness were prepared and tested under uniform moment loading (Table 4). Laterally unbraced lengths of the test specimens were controlled such that inelastic LTB could be induced.

3.2. Test Results and Key Observations

All specimens exhibited LTB strength exceeding the nominal strength according to current AISC provisions by a sufficient margin as shown in Fig. 7. Especially, specimens S2 and S3 in Group A reached a rotation capacity required for plastic design, although their laterally unbraced length was longer than L_p (Fig. 8).

Group B specimens showed earlier post-buckling strength degradation and low rotation capacity. The strain measurements at the top (compression) flange indicated that more rapid and severe out-of-plane distorsion of the compression flange occurred in specimens with high D/B ratio, thus inducing more severe post-buckling second order effect. More comprehensive investigation of inelastic LTB of high-strength steel beams as affected by sectional geometric configuration can be found in the recent study by Park (2015).

4. Concentric and Eccentric Load Tests of Stub Columns

A total of 10 high-strength steel (HSA800) box, cruciform, and H-shaped stub columns were tested to evaluate the uniform compression and *P-M* interaction strength (Kim et al., 2014). Seven stub columns of ordinary steel (SM490) were also tested for comparison purposes. With the plate-edge restraints and plate slenderness as the key variables, the primary objective was to evaluate if the AISC local buckling provisions are also applicable for 800 MPa high-strength steel. Together with the observations made from residual stress measurements and a comparison with test results by others, the following conclusions were drawn.

All 800 MPa specimens with stiffened element, unsti-

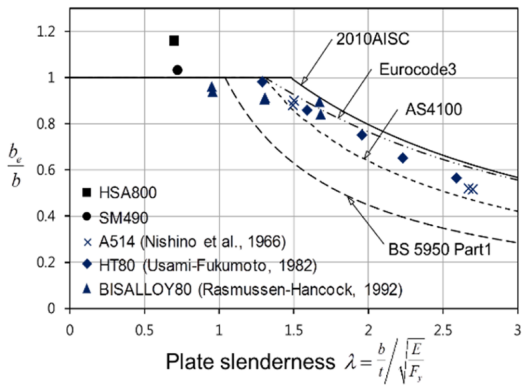

(a) Box specimens

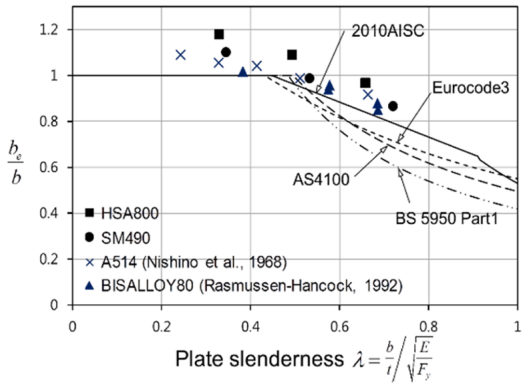

(b) Cruciform specimens

Figure 11. Comparison with previous test results and various design standards.

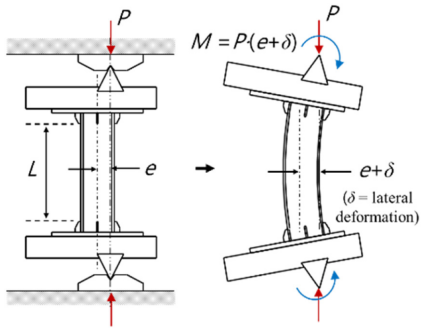

Figure 12. Test setup for eccentric load tests.

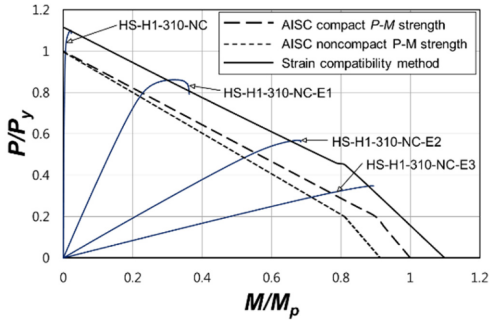

Figure 13. Comparison of experimental and AISC P-M interaction strength.

ffened element, and combination of both, designed according to the local buckling criteria of the 2010 AISC Specification, exhibited sufficient strength under uniform compression, and generally outperformed ordinary steel (SM 490) specimens (see Figs. 9~11). However, for stiffened elements under uniform compression, many of test data from previous researches, which also used high-strength steels of a strength grade similar to HSA800, often showed less strength than the nominal level specified by the 2010 AISC Specification and Eurocode 3.

The experimental *P-M* interaction strength obtained from the eccentrically loaded specimens with noncompact flange showed strength much higher than the AISC nominal *P-M* strength (see Figs. 12~13). Actually, all the specimens exhibited the *P-M* interaction strength exceeding the AISC "compact-section" *P-M* interaction strength. The experimental *P-M* interaction strength was very accurately predicted with the strain compatibility method by using the measured stress-strain curve, or by explicitly considering early strain-hardening property of high strength steel.

Many steel design codes assume that the residual stress is proportional to the yield stress of base metal. However, the residual stresses distribution measurement (Lee et al., 2013; Kim et al., 2014) again confirmed that the magnitude of the residual stress is virtually independent of the yield stress of the base metal, implying that the impact of residual stress on inelastic buckling of high-strength steel is less. Inelastic buckling tests on HSA800 intermediate columns were also conducted and the measured buckling strength exceeded the nominal strength of the AISC Specification (not shown here).

5. Seismic Tesing of Welded Moment Connections

As noted above, all the high-strength steel beams did not meet the rotation capacity requirement implied for high seismic application (R>7). However, the rotation capacity of 7 often implied for high seismic application following Chopra and Newmark (1980) should be considered as the very qualitative and judgmental postulation in the past. The relation among system, story and member ductility in steel moment frames can vary significantly from design to design and is very difficult to set forth definitively. Further, seismic applicability of any steel material nowadays should be evaluated based on the cyclic seismic testing of connection assembly, not just member testing, according to some well-established seismic loading protocol (for example, 2010 AISC Seismic Provisions).

On the other hand, because of concerns about low ductility, weldability as well as lack of test data, the yield stress

Table 5. Summary of cyclic test results

Specimen	Loading Direction	Initial Stiffness (kN/mm)	Yield rotation angle (rad)	Plastic moment (kN·m)	Maximum rotation angle (rad)	Maximum moment (kN·m)	Plastic rotation angle (rad)
Scallop	Positive(+)	11.24	0.0218	3003	0.0320	3411	0.0102
	Negative(-)	11.25	0.0233	3213	0.0296	3504	0.0063
Non-Scallop	Positive(+)	11.52	0.0225	3176	0.0415	3831	0.0190
	Negative(-)	10.84	0.0262	3476	0.0430	4088	0.0186

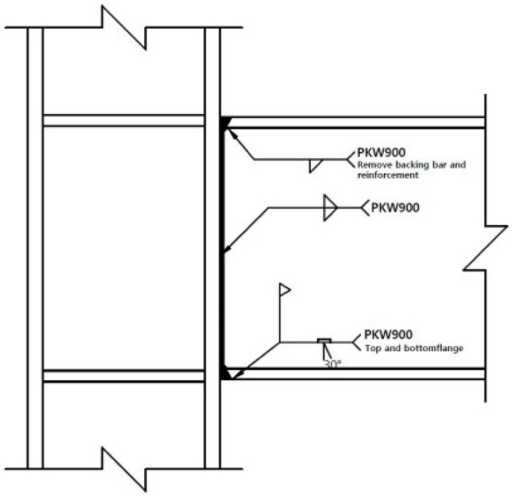

Figure 14. Non-scallop beam-to-column welded joint.

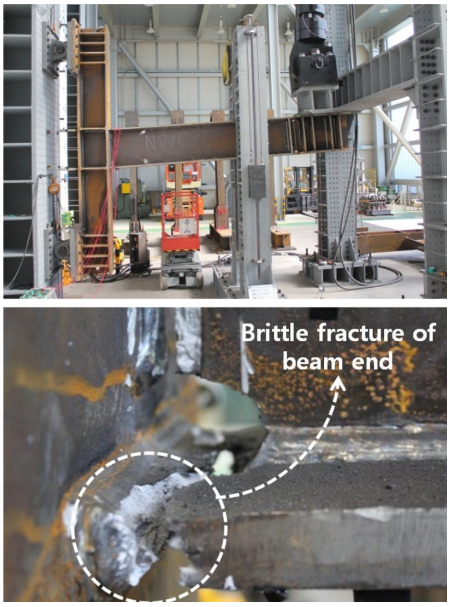

Figure 15. Overall view of ultimate deformation and beam bottom flange fracture (non-scallop specimen).

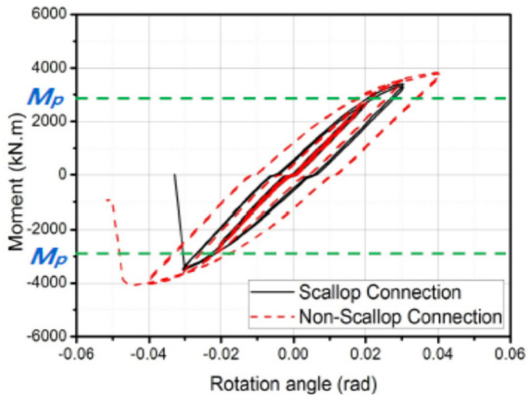

Figure 16. Comparison of cyclic responses.

of steel is limited to 345 MPa (50 ksi) for "inelastic" beams and 450 MPa (65 ksi) for "elastic" columns, respectively in the 2010 AISC Seismic Provisions if the suitability of the steel material is not determined by testing or other rational criteria. Although the best use of HSA800 members in the seismic force resisting system is for the elastic elements according to the capacity design concept, research engineers in RIST (Kim, 2015) conducted cyclic seismic testing of welded beam-to-column subassemblage fabricated of HSA800. Two specimens composed of a H-600×200×15×25 beam (HSA800) and a H-440×440×25×35 column (HSA800) were tested according to the AISC seismic cyclic testing procedure. They were nominally identical except the beam-to-column welding details as shown Fig. 14. In one specimen, the non-scallop welding detail proposed in Japan after the 1995 Kobe earthquake was used. The newly developed FCAW electrode named PKW 900 (equivalent to E125T1-G) was used in fabrication. The tensile strength and the CVN toughness of PKW900 was 900 MPa and 47J@-5°C, respectively. It should be noted that the CVN toughness of 47J@-5°C is much lower than the min. level of 27J@-29°C recommended for seismic application nowadays.

All inelastic deformation was developed in the beam because the panel zones and the columns were sufficiently strong compared to the beam. Both tests were terminated due to the brittle fracture of beam bottom flange close to the CJP weld (see Fig. 15). As shown in Fig. 16 and Table 5, the non-scallop specimen performed better and the connection plastic rotation achieved were about 2% radians (or between IMF and SMF level), although the yield stress was almost two times higher than the AISC upper limit 345 MPa (50 ksi) and the welding electrode used was not tough enough. These test results again confirm the well-

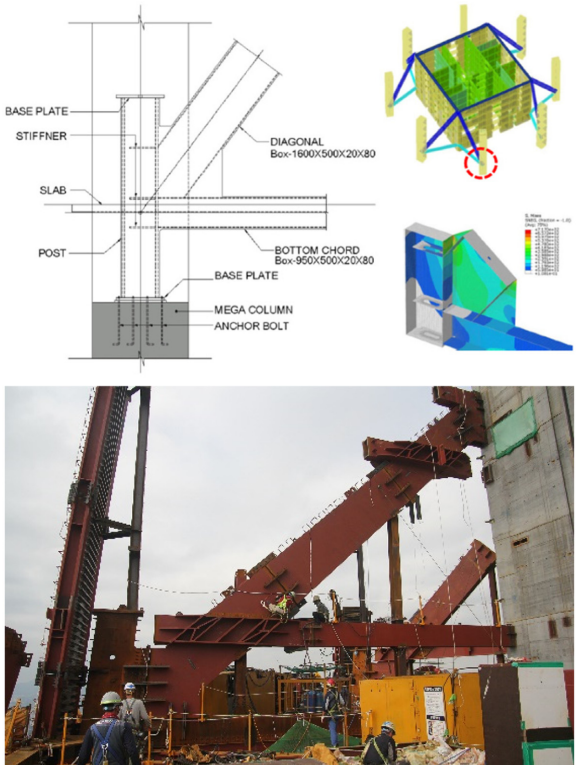

Figure 17. Outrigger-to-mega column connecting box built-up from HSA800.

known fact that joint detail itself is also a crucial determinant for connection cyclic rotation capacity. Although test data is limited, these test results seem to indicate that HSA800 members have the potential to be used as non-ductile members or members with limited ductility demand in many seismic load resisting systems if connections are well-designed.

6. Recent Application Examples

HSA800 also underwent extensive welding test for qualification as high performance steel. Currently, HSA800 in Korea is mainly being applied to highrise or mega building structures because of reduced steel tonnage, reduced welding sizes, reduced individual piece weights, and smaller piece sizes. In some case, lifting issue often dictated the use of HSA800 members.

The construction of Lotte World Tower, located near Han River in Seoul, 123 story-high and 555 meters tall, has been completed early this year. HSA800, offered as a new steel material during construction, was just selectively applied to this tower. The lateral-load resisting system is consisted of core wall, 2 outriggers, 2 belt trusses and 8 mega columns. Wind was the governing lateral load in most cases since Korea is not so seismically active and the period of the building is very long, about 10 sec. When the author was structurally involved in this project, the

Figure 18. Core-wall embedded plates designed using HSA800.

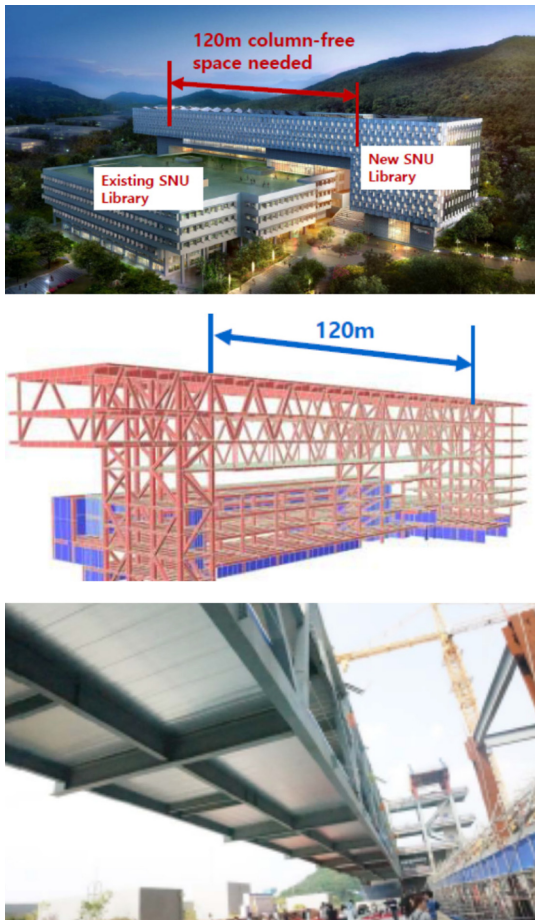

Figure 19. New SNU library mega truss frame system fabricated from HSA800.

first mission was to propose an idea to replace outrigger-to-mega column connecting assembly, originally proposed as very expensive casting type, with less expensive built-up box. The casting-based connecting assembly originally offered was as follows: weight = 13 ton, height = 3 m, width = 1 m, variable thickness up to 230 mm. Further,

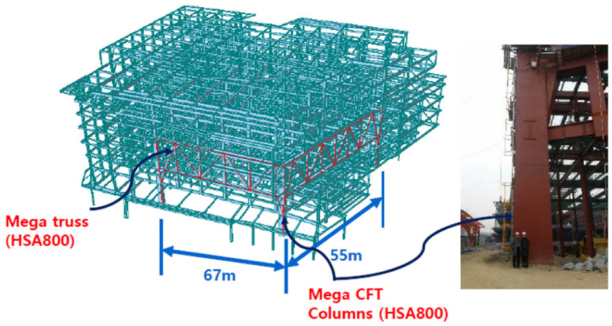

Figure 20. Application of HSA800 to transportation complex building in Dae-gu city.

foreign technology was mandatory. The author proposed a cost-effective HSA800 built-up box, and was accepted and actually built (see Fig. 17). The author noted that the major load path is through the web of the outrigger, and the three-sided welded horizontal stiffener with gap, opposite to the outrigger, is acceptable, thus avoiding costly electro-slag welding. The gap can be used as a hole to monitor concrete compaction. The FE analysis also supported this proposal. The wall thickness was reduced to 60 mm by using HSA800. The built-up cost was just about 30% the casting detail originally proposed.

The embedded plates at one end of outriggers were designed using HSA800 such that the plates could be easily accommodated within the core wall (see Fig. 18). Many mega members such as outriggers and four-story high belt trusses supporting uppermost lantern structure and hotel columns could be re-designed by using HSA800. But structural designers did not want to change the original SM570 TMC-based design because wind tunnel test were already done based on the original design.

Because new SNU library was designed to be built partially over the roof of existing SNU library, 120 m-long column free space was needed. The cost-effective solution adopted was to use mega truss system composed of box members fabricated of HSA800 (see Fig. 19). This building is the first one which used HSA800 in all frame members.

Fig. 20 shows the 3-D frame model of the transportation complex building in Dae-gu City and the location of the mega trusses and mega CFT columns built up from HSA 800. Existing subway route dictated very long spanning structures. Mega trusses and mega CFT columns fabricated from HSA800 were used to meet the spanning requirement. In this project, HSA800 was especially welcomed because of the advantage in lifting.

7. Summary and Conclusions

Main conclusions drawn from a series of tests and related analytical studies on 800 MPa high-strength steel members can be summarized as follows.

(1) 800 MPa specimens designed according to the FLB criteria of the AISC Specification developed a sufficient strength for elastic design and a marginal rotation capacity for plastic design.

(2) By using a simplified inelastic curvature distribution for a steel beam under a moment gradient, it was clearly shown that, without introducing distinct and significant yield plateau to the stress-strain property of high-strength steel, it is inherently difficult to achieve a high rotation capacity even if all the current AISC stability limits are met.

(3) All 800 MPa specimens with stiffened element, unstiffened element, and combination of both, designed according to the local buckling criteria of the AISC Specification for uniform compression, exhibited sufficient strength and generally outperformed ordinary steel specimens.

(4) The experimental *P-M* interaction strength obtained from the eccentrically loaded specimens with noncompact flange was much higher than the AISC nominal *P-M* strength.

(5) Many steel design codes assume that the residual stress is proportional to the yield stress of base metal. However, the measured residual stresses distribution again confirmed that the magnitude of the residual stress is virtually independent of the yield stress of the base metal, implying that the impact of residual stress on inelastic buckling of high-strength steel is less.

(6) All HSA800 specimens exhibited LTB strength exceeding the AISC nominal strength by a sufficient margin. Specimens with high warping showed earlier post-buckling strength degradation and low rotation capacity because of more rapid and severe out-of-plane distorsion of the compression flange after buckling initiation.

(7) Cyclic seismic testing of this study showed that HSA 800 members have the potential to be used as non-ductile members or members with limited ductility demand in many seismic load resisting systems if connections are well-designed.

(8) Currently, HSA800, which underwent extensive structural testing for qualification as high performance steel, is mainly being applied to highrise or mega building structures, often selectively, because of reduced steel tonnage, reduced welding sizes, reduced individual piece weights, and smaller piece sizes.

Acknowledgement

Support to this study by the POSCO Affiliated Research Professor Program is gratefully acknowledged.

References

AISC. “Specification for structural steel buildings,” AISC, Chicago, IL, (2010a).

AISC. “Seismic provisions for structural steel buildings,” AISC, Chicago, IL (2010b).

Chopra, A. K., and Newmark, N. M., “Design of earthquake

resistant structures," Wiley, New York (1980).
de Normalización, C. E. (Ed.). "EN 1993-1-1: Eurocode 3: Design of Steel Structures- Part 1-1: General Rules and Rules for Buildings ," Comité Europeo de Normalización, Brussels, (2005).
Galambos, T. V., Hajjar, J. F., and Earls, C. J., "Required properties of high-performance steels," Report No. NISTIR 6004, NIST (1997).
Green, P. G., "The inelastic behavior of flexural members fabricated from high performance steel," Ph.D. Dissertation, Lehigh University, Bethlehem, PA (2000).
Kemp, A. R., "Inelastic local and lateral buckling in design code," *J. Struct. Eng.*, ASCE, 122(4), April, pp. 374-382 (1996).
Kim, D.-K., Lee, C.-H., Han, K.-H., Kim, J.-H., Lee, S.-E., and Sim, H.-B., "Strength and residual stress evaluation of stub columns fabricated from 800 MPa high-strength steel", *Journal of Construction Steel Research*, Vol. 102, pp. 111-120 (2014).
Kim, J.-W., Cyclic Seismic Testing of HSA800 Beam to Column Welded Moment Connections, Technical Repot, RIST, Korea (2015).
Lay, M. G., "Yielding of uniformly loaded steel members," *J. Struct. Div.*, ASCE, 91(ST6), Proc. Dec., pp. 49-66 (1965b).
Lee, C.-H., Han, K.-H., Uang, C.-M., Kim, D.-K., Park, C.-H., and Kim, J.-H., "Flexural Strength and Rotation Capacity of I-Shaped Beams Fabricated from 800-MPa Steel," *J. Struct. Eng.*, ASCE, 139(6), pp. 1043-1058 (2013).
McDermott, J. F., "Plastic bending of A514 steel beams," *J. Struct. Div.*, ASCE. 95 (ST9), Sep., pp. 1851-1871 (1969).
Park, C.-H., "Inelastic Lateral-torsional Buckling of High-strength Steel I-shaped Flexural Members", Ph.D. Dissertation, Seoul National University, Seoul, Korea (2015).
Park, C.-H. and Lee, C.-H., "Laterally Unbraced Length for Preventing Inelastic Lateral-Torsional Buckling of High-Strength Steel Beams," PSSC 2013, Singapore (2013).
Ricles, J.M., Sause, R., and Green, P.S., "High-strength steel: Implications of material and geometric characteristics on inelastic flexural behavior," *J. Eng. Struct.*, 20(4-6), pp. 323-335 (1998).
Han, K.-H and Lee, C.-H., "Elastic Flange Local Buckling of I-Shaped Considering Effect of Web Restraint", *Thin-Walled Structures*, 105, pp. 101-111 (2016).